Singlet fission in heterogeneous lycopene aggregates

Vasyl Veremeienko, Chloe Magne, Minh-Huong Ha-Thi, Ana A Arteni, Andrew A Pascal, Mikas Vengris, Thomas Pino, Robert Bruno, Manuel J. Llansola-Portoles

Singlet fission in heterogeneous lycopene aggregates

Vasyl Veremeienko[a†], Chloe Magne[a†], Minh-Huong Ha-Thi[b], Ana A. Arteni[a], Andrew A. Pascal[a], Mikas Vengris[c], Thomas Pino[b], Bruno Robert[a], Manuel J. Llansola-Portoles[a*]

[a] Université Paris-Saclay, CEA, CNRS, Institute for Integrative Biology of the Cell (I2BC), 91198, Gif-sur-Yvette, France.

[b] Université Paris-Saclay, CNRS, Institut des Sciences Moléculaires d'Orsay, 91405, Orsay, France.

[c] Laser Research Center, Faculty of Physics, Vilnius University, Sauletekio Ave. 10, LT-10223, Vilnius, Lithuania.

† These authors contributed equally to this work

* Corresponding author

e-mail: manuel.llansola@i2bc.paris-saclay.fr

Keywords: self-assembled lycopene, singlet exciton fission, resonance Raman, transient absorption

Abstract

We have prepared lycopene aggregates with negligible scattering in an acetone-water suspension. The aggregates exhibit highly distorted absorption, extending from the UV up to 568 nm, as a result of strong excitonic interactions. We have investigated the structural organization of these aggregates by resonance Raman and TEM, revealing that the lycopene aggregates are not homogeneous, containing at least five different aggregate species. Transient absorption measurements upon excitation at 355, 515, and 570 nm, to sub-select these different species, reveal significant differences in dynamics between each of the aggregate types. The strong excitonic interactions produce highly distorted transient electronic signatures, which do not allow an unequivocal identification of the excited states at times shorter than 60 ps. However, these experiments demonstrate that all the lycopene aggregated species form long-living triplets *via* singlet fission.

Introduction

Carotenoids are a large family of tetraterpenoid derivatives present in every biological kingdom. They have a wide variety of roles, notably in providing colours in a range of complex signalling processes, quenching reactive oxygen species, and enhancing light-harvesting efficiency in photosynthesis[1]. Carotenoids have remarkably complex excited-state manifold and dynamics. The lowest-lying excited state, S_1 ($2^1A_g^-$), is absorption-silent, displaying the same symmetry as the ground state S_0 ($1^1A_g^-$) [2]; the strong absorption of carotenoids arises from a transition from S_0 to the second excited state, S_2 ($1^1B_u^+$). The energy of the $S_0 \rightarrow S_2$ transition depends on the length of the C=C conjugated chain, as well as on the polarisability of the environment[3, 4]. In the simplest cases, this excited S_2 state decays by internal conversion (<200 fs) to S_1, which itself decays to the ground-state S_0 by internal conversion in several picoseconds[5-7]. However, further "dark" states, such as S*, are proposed to account for the intricate network of relaxation pathways observed[8-11]. In monomeric carotenoids, the ultrafast deactivation of the excited states prevents the formation of triplets *via* intersystem crossing. Aggregated carotenoids, on the other hand, are able to generate triplets in an ultrafast manner through singlet fission. Carotenoids constitute the only known family of natural molecules capable of singlet fission in both artificial aggregates [12-19] and biological systems like photosynthetic antennae[20-22] or chromoplasts[23, 24].

The mechanisms governing singlet fission in synthetic compounds such as acenes and rylenes is reasonably well understood[25-27]. However, there is a lack of consensus on the mechanisms and even the excited states involved for this process in carotenoids. For zeaxanthin aggregates created by adding water to organic solvent, for example, S_2 has been proposed as the parent state for triplet formation[18], whereas a hot-S_1 state is proposed for zeaxanthin aggregates in ethanol/THF [17]. Zeaxanthin in lipid membranes forms triplets in a few ps, suggesting S_1/S^* as the parent state[28]. For β-carotene aggregates, the triplet parent state is attributed to S_2 for β-carotene micelles [16], whereas the attribution was inconclusive for β-carotene aggregates in bovine serum [15]. Astaxanthin aggregates in acetone/water mixtures are proposed to have the S_2 state as triplet parent[13], but no conclusions could be drawn for its aggregates in hydrated dimethyl sulfoxide, despite their absorption spectra being similar[29]. Fucoxanthin aggregates prepared in DMS/water or ethanol/water mixtures exhibit different time evolution with changes of excitation wavelength from 460nm to 440 nm[14]. Finally, lycopene aggregates have been proposed to have S* as a parent state [12]. The discrepancies are also extended to singlet fission in natural systems, where S* has been proposed for long carotenoids in photosynthetic proteins [20-22], the vibrationally hot-S_1 for daffodil chromoplasts[24], and an unknown S-like state for tomato chromoplasts[23].

Treatment of the carotenoid aggregates as a single entity with just one set of spectroscopic properties may be one of the causes of these contradictory results. It is well known that changing the preparations conditions (e.g. temperature, solvent mixture, etc…) produces carotenoid aggregates with different properties. However, a few studies have shown that each of the samples obtained using various protocols may contain more than one species of aggregate. These include characterization by resonance Raman of daffodil chromoplasts[24] and transient absorption spectroscopy in astaxanthin aggregates[13] and zeaxanthin aggregates[18]. Failure to consider that samples may contain a mixture of different carotenoid aggregates with different properties may lead to incorrect conclusions. Carotenoids are known to change their energetic relaxation pathways dramatically upon minor changes in conformation (e.g. photosynthetic proteins)[30, 31]. The diversity of interpretations could also arise from an oversimplified classification of the aggregates. The traditional description for aggregates relies on Kasha theory[32], where J- and H-aggregates are assigned on the basis of red or blue absorption shifts, respectively. However, it is currently accepted that this absorption shift is not a strong marker for describing the type of aggregates[33]. For example, helically-organized H-aggregates of lutein derivatives present a large blue shift for strong excitonic

interactions (short molecular distance), and gradually redshift with changes in the molecular distance and twisting angle[34]. Such red-shifted H-aggregates would previously have been identified (incorrectly) as J-aggregates[35, 36]. Moreover, modelling approaches which take into account vibronic coupling and intermolecular charge transfer have shown that the characterization of aggregates and their excited state manifold is far more complex than the binary H/J determination, namely: Hj-, hJ-, or Herzberg–Teller J/H-aggregates[33]. The lack of a description of the excited state manifold for carotenoids makes the creation of a model a daunting task.

In this work, we aim to highlight the importance of a detailed characterization of carotenoid aggregate species. We have chosen lycopene as the study case, since the assignments found in the literature are contradictory (J-aggregates[23], H-aggregates[12], and a mixture of H- and J- aggregates [37-39]). The lycopene molecule has a flat structure, in contrast to bulkier carotenoids with twisted terminal rings or keto groups, which allows close contact between the conjugated chains of neighbouring molecules (3.3 Å)[36], and may permit several structural organizations. We have produced lycopene aggregates in stable acetone-water suspension with low scattering, allowing us to perform spectroscopic measurements in the UV region of the spectrum - which had proved inaccessible using crystalloid films[23] or lycopene nanoparticles[12]. We characterize their absorption and morphology, and, using resonance Raman, we demonstrate the presence of different types of aggregate in the sample, and assess their configuration. We then use femtosecond-to-microsecond transient absorption spectroscopy, revealing the process of singlet fission in action in the UV-region with unprecedented resolution.

Experimental

Preparation of lycopene aggregates. Tomato paste was used as raw material to obtain monomeric lycopene, extracted and purified as described elsewhere[23]. Briefly, tomato paste was mixed with ethyl acetate (vol. 50/50) and stirred continuously for 60 minutes at room temperature; the liquid fraction (ethyl acetate) was then decanted off and the remaining solids were re-extracted in fresh solvent, repeating the extraction/decanting cycle three times. The organic fraction, containing mainly lycopene, β-carotene and chlorophyll, was dried with a rotary evaporator at 40º C. Lycopene was separated from other compounds on a silica gel column, using 100 % n-hexane as mobile phase. In these conditions, lycopene is eluted first followed by β-carotene, whereas the chlorophyll fraction remains on the column. The purified lycopene fraction from the chromatographic

column was dried with a rotary evaporator at 40 º C, and stored at -20 º C until further use. We improved the protocol to generate reproducible lycopene aggregates with low scattering, and high stability in suspension, as follows: 50mg/L lycopene in absolute acetone (≥ 99%) was added dropwise to distilled water (Millipore system 18.2 Ω cm) under weak sonication at room temperature, to reach an acetone/water ratio of 80/20 (v/v). The aggregate solution (ca. 25mg/L) was kept under sonication for 30 min, until the absorption remains stable.

UV-Vis Absorption spectra were measured on a Varian Cary E5 Double-beam scanning spectrophotometer (Agilent), using a 4 mm path-length cuvette.

Electron microscopy. The samples for electron microscopy were negatively stained with 2 % uranyl acetate (w/v) on glow-discharged, carbon-coated copper grids. Data collection was performed using a Tecnai Spirit transmission electron microscope (TFS) equipped with a LaB6 filament, operating at 100 kV. Images were recorded on a K2 Base camera (Gatan/Ametek, 4kx4k) at 21000 or 4400 magnification (pixel size at specimen level – 1.9 and 0.83 nm, respectively).

Resonance Raman spectra were recorded at room temperature and 77 K, with laser excitations obtained from Coherent Ar+ (Sabre) and at 577.0 nm with a Genesis CX STM laser (Coherent). Output laser powers of 10–100 mW were attenuated to < 5 mW at the sample and using unfocused laser beams. Scattered light was collected at 90° to the incident light, and focused into a Jobin-Yvon U1000 double-grating spectrometer (1800 grooves/mm) equipped with a red-sensitive, back-illuminated, LN2-cooled CCD camera. Sample stability and integrity were assessed based on the stability of the Raman signal.

Nano-to-millisecond transient absorption experiments were performed on a home-made nanosecond transient absorption setup, using a broadband OPO (optical parametric oscillator, ~4 ns temporal width) as pump laser, pumped by the 3rd harmonic of a Nd:YAG laser. A LEUKOS STM-2-UV super continuum laser (350-2400 nm, <1 ns temporal width) was used as probe laser. A system of lenses and mirrors shape the laser beams for maximum, homogeneous overlap on the sample. Analysis of the excited-state dynamics of self-assembled lycopene was performed using excitation at 570 nm, with an energy of 1.2 mJ per pump pulse. The frequency of the pump pulse was set at 10 Hz, while that of the probe pulse was reduced to 20 Hz using a rotating chopper. The sample was installed at ~45° relative to the pump and probe beams. After passing through the sample, the probe pulse was injected into a bundle of optical fibres (200 μm core), whose round entrance cross-section

transitioned to a linear alignment at the exit in order to fit the entrance of the spectrometer. The latter was in turn coupled with an intensified charge coupled device (ICCD) camera. A reference spectrum of the probe was measured for each laser pulse, allowing correction for fluctuations. The time delay between pump and probe pulses was synchronized electronically through an in-house electronic pulse generator, to monitor temporally- and spectrally-resolved absorption spectra.

Femto–to–nanosecond time-resolved transient absorption spectra were recorded on a commercial transient absorption spectrometer (Harpia, Light Conversion). Pump and probe pulses for the spectrometer were derived from an amplified Ti:Sapphire laser (Libra, Coherent). Tunable pump pulses with center wavelength at 490 nm were obtained from an optical parametric amplifier (Topas-800, Light Conversion). A white light continuum, used to probe the absorption changes in the 350-750 nm range, was generated in CaF_2 from the fundamental output of the laser. The time resolution of the instrument is ca. 120 fs. Excitation energies were set to approximately 600 nJ pulse.

Global analysis of time-resolved spectra was performed using commercial CarpetView data analysis software (Light Conversion).

Results

The absorption spectrum of monomeric lycopene in *n*-hexane exhibits three sharp bands, located at 442.4, 470.4 and 501.7 nm, respectively, corresponding to the 0-2, 0-1 and 0-0 vibronic levels of the $S_0 \rightarrow S_2$ electronic transition (figure 1, solid blue line). These absorption transitions redshift with increasing polarizability of the environment, the 0-0 transition reaching 543 nm in carbon disulfide (figure 1, dotted blue line)[4]. Lycopene aggregates (red curve in figure 1) display a very different absorption spectrum, featuring a pronounced band peaking at 355 nm with a shoulder around 375 nm, then two bands at *ca* 414 & 481 nm, and a very redshifted band at 568 nm. A long absorption tail extending up to 700 nm is also visible. Lycopene aggregates, prepared by different protocols or formed naturally in chromoplasts, lead invariably to similar spectral features, as previously observed in tomato chromoplasts[23, 37], lycopene films[23], and lycopene crystalloids[37, 38]. There is a consensus that these features are due to excitonic interactions[40, 41], but no clear description of the origin of these bands has been proposed. The peak at 355 nm is an unmistakable signature of lycopene forming strong excitonic interactions in H-type aggregates, whereas the bands with small blue or red shifts (481 & 514 nm) and the largely redshifted 568 nm band remain controversial.

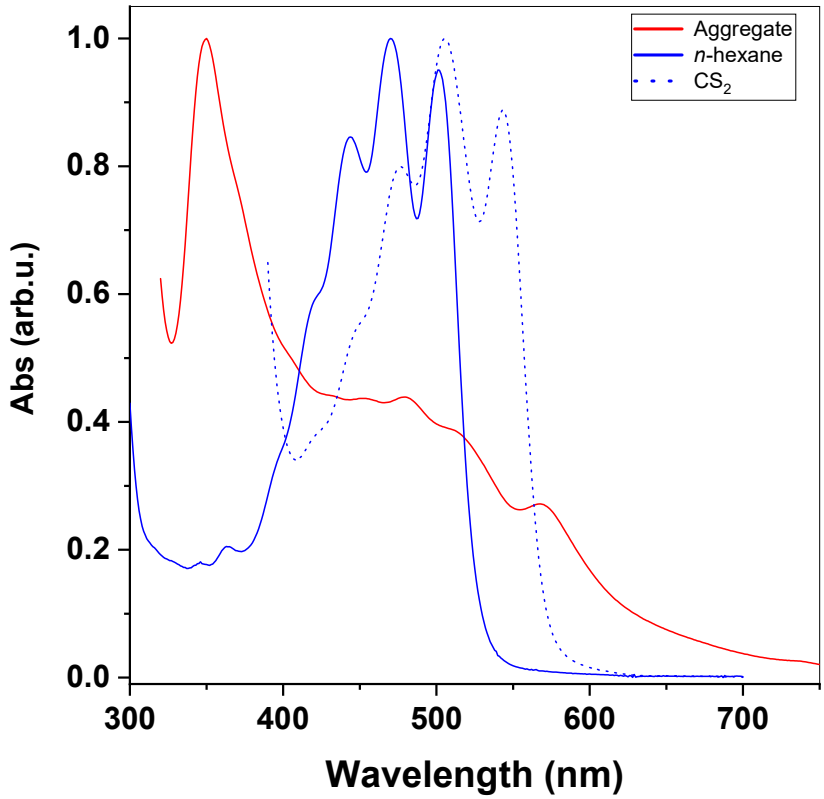

Figure 1| Room temperature absorption spectra of monomeric lycopene in n-hexane (solid blue line), in CS2 (dotted blue line), and lycopene aggregates in acetone: water 1:1 suspension (solid red line).

Resonance Raman scattering spectroscopy is a highly sensitive tool to investigate multiple species in a complex matrix. In the *resonance* condition, when the energy of the incident light matches the electronic transition of a sub-population in the complex mixture, contributions from this subset of molecules may be selectively observed, and the narrowing of the electronic transitions at low temperatures increases this selectivity[42, 43]. This technique thus allows for the observation of the vibrational properties of different lycopene species in a mixture, provided that they display different absorption properties. Resonance Raman spectra of carotenoids contain four main groups of bands, ν_1 through ν_4, each providing specific information on the conformation and/or configuration of the scattering molecule(s)[3]. In the high-frequency region, the intense ν_1 band around 1500-1530 cm^{-1} arises from stretching vibrations of the conjugated C=C bonds in the polyene chain. In carotenoid monomers, its precise frequency depends on the effective conjugation length of the molecule[4], which is related to the energy of the ground-state. In aggregates, it can be used to probe intermolecular interactions, on the basis of their ground-state properties[40]. The group of bands around 1160 cm^{-1}, called ν_2, arises from stretching vibrations of C-C bonds coupled with C-H in-plane bending modes.

These modes constitute a fingerprint region for determining carotenoid isomerization states (*trans*/*cis*)[44-46]. The ν_4 mode around 960 cm^{-1} arises from C-H out-of-plane wagging motions coupled with C=C torsional modes[47], and this region is an indicator of out-of-plane distortions of the carotenoid conjugated chain[47, 48].

The 77 K resonance Raman spectrum of lycopene in diethyl ether (polarizability 0.230) is shown in figure 2a. The ν_1 band is observed at 1517 cm^{-1}, a frequency expected for a carotenoid containing eleven conjugated C=C bonds (it may downshift up to 2 cm^{-1} for highly polar solvents). The ν_2 region displays a main band at 1155 cm^{-1} and is typical for lycopene in the all-*trans* configuration. Finally, the ν_4 region exhibits a small, structure-less envelope characteristic of carotenoid in a relaxed conformation in solution. Figure 2b shows the equivalent spectrum for lycopene aggregates measured using five different excitation wavelengths (363.8, 488.0, 501.7, 514.5, and 577.0 nm) (for room temperature resonance Raman, see supporting information, figure S1). The position of the ν_1 band of lycopene aggregates exhibits a clear dependence on the excitation wavelength, peaking at 1511, 1529, 1526, 1522 & 1511 cm^{-1} for 363.8, 488.0, 501.7, 514.5, & 577.0 nm excitation, respectively. At 488.0, 501.7 and 514.5 nm, it is accompanied by a small shoulder at 1511 cm^{-1} whose intensity decreases as the excitation moves to the red. Monomeric lycopene may absorb at 488.0, 501.7 and 514.5 nm, but the position of the corresponding ν_1 bands (1529, 1526, and 1522 cm^{-1}) are shifted to higher frequencies relative to lycopene in ethyl acetate (1517 cm^{-1}), indicating that no lycopene monomers are present in the sample[4]. The ν_2 region retains the characteristic profile of all-*trans* lycopene, indicating that the aggregation process induces no isomerization of the molecule. The ν_4 region exhibits sharp vibrational modes at 953, 958, and 966 cm^{-1} for 577.0 nm and 363.8 nm (although 966 cm^{-1} is somewhat obscured by the solvent band for 363.8 nm excitation). The vibrational modes in the ν_4 region observed for 514.5 nm excitation are significantly lower in intensity, and appear at 950, 955, and 963 cm^{-1}. The absorption at 514 nm thus arises from a different lycopene species, for which the packing twists/bends their backbone to a lesser extent and induces a different configuration (different position of the vibrational modes). The ν_4 regions observed for 488.0 nm and 501.7 nm excitation are similar to carotenoids in solution, indicating the presence of carotenoids with an unstrained conformation in these aggregates.

The resonance Raman data thus reveal the presence of several different lycopene aggregated species. Three different species are responsible for the absorption bands at 488.0, 501.7 and 514.5 nm, referred to below as species 1, 2 and 3, respectively. The species 1 & 2 are in a relaxed

conformation, whereas species 3 is somewhat twisted/bent. Assignment of the absorption bands at 355 and 568 nm needs a more detailed analysis. The same ν_1 frequency (1511 cm^{-1}) is observed for excitations in both transitions (363.8 and 577.0 nm, respectively). This could imply that these bands are two different electronic transitions of the same species. While the ratio between the ν_3 band at 1005 cm^{-1} and the band at 958 cm^{-1} appears different between 577.0 and 363.8 nm excitation, this could originate from the different excited states used to induce resonance. These spectra can thus be interpreted in two ways. First, only one strongly-coupled H-type species is present in the mixture (species 4), corresponding to a highly twisted/bent lycopene displaying two electronic transitions at 577.0 & 363.8 nm. Alternatively, two strongly-coupled H-type species are present in the sample (species 5 & 6), absorbing at 355 and 568 nm, respectively, with the former packing the lycopene in a somewhat more relaxed conformation than the latter. Species 1, 2 & 3 (as well as species 6 if there) can be assigned to helical organizations of H-type aggregates, which have been shown to produce an absorption redshift depending on the twisting angle[34]. Species 5, if present, would correspond to pure H-type aggregates with a strong absorption blue-shift. On the other hand, the possibility of species 4, presenting absorption at 577.0 nm and 363.8 nm, is highly puzzling. Although carotenoid H-aggregates have been reported with similar electronic transitions, it was never formally shown that both transitions arose from the same aggregate, as the homogeneity of the aggregate preparation was not verified. We propose that the characteristics of species 4 would correspond to the properties predicted by calculations obtained for medium-strength coupled H-aggregates in carotenes[34], where there is a main blue-shifted absorption, along with a weak red-shifted peak arising from Herzberg −Teller coupling (considered as a forbidden transition for H-aggregates) [33]. Note that from these Raman spectra, we can only determine the *minimum* number of species present in the sample, and cannot exclude the existence of any number of minor species we do not detect.

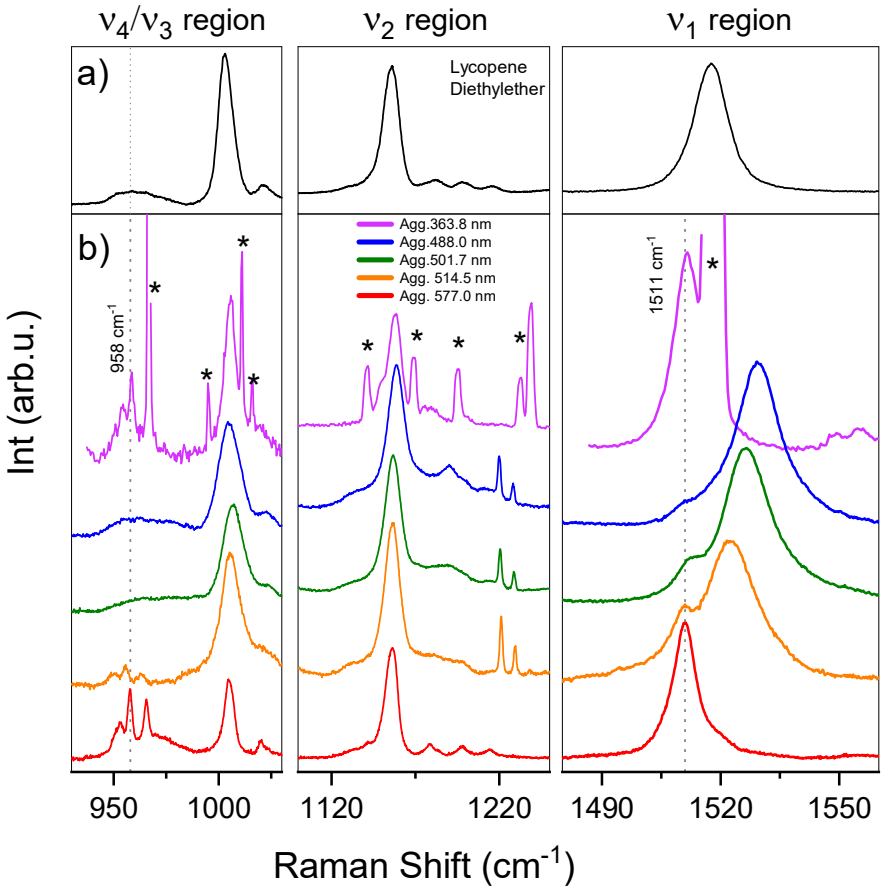

Figure 2| Resonance Raman spectra at 77 K of lycopene monomer in diethyl ether (a), and lycopene crystalloids excited at 363.8, 488.0, 501.7, 514.5 & 577.0 nm – asterisks mark acetone solvent bands (b).

Transmission electron microscope (TEM) images of lycopene aggregates appear to indicate at least two different aggregate morphologies (figure 3) – a crystal-like rod structure (length 2 μm and diameter 100 nm) and a more irregular geometry (diameter 50-200 nm). This is the first time that small, stable lycopene assemblies in solution have been characterized by TEM at high concentration (ca. 10^4 M). Small rod-like structures have been found for three different H-aggregates of zeaxanthin[41]. It was proposed that the OH groups on the terminal rings of zeaxanthin and lutein facilitate the organization of these aggregates[34, 41]. The lack of any such groups in lycopene should thus increase the possibility of different types of association. The observed crystal-like morphologies are disordered, and do not allow a prediction to be made about the symmetry of the unit cell. TEM images do not contain enough information to determine whether each structure contains one single lycopene organization, or there are several sub-domains within the same aggregate.

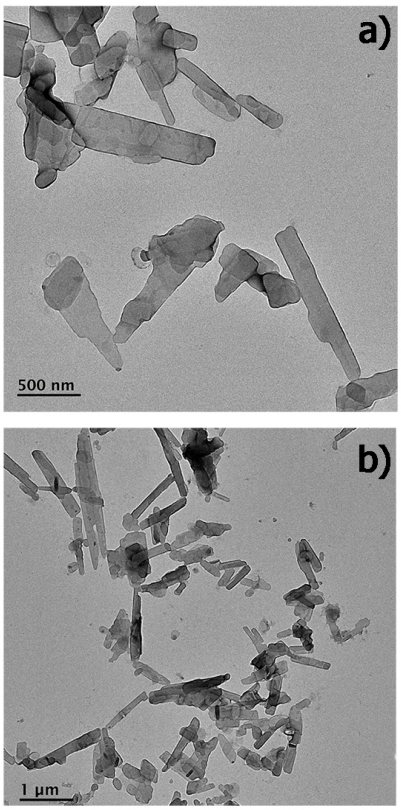

Figure 3| TEM of lycopene aggregates at two different magnifications: scale bar **a)** 500, and **b)** 1 µm.

Femtosecond-to-nanosecond transient absorption data were obtained to investigate the photochemistry of the three populations of lycopene aggregate detected by resonance Raman (363.8 nm, 514.5 nm, and 577.0 nm). An overview of the dataset acquired at 355 nm excitation is presented in Figure 4A, along with kinetic traces measured at selected wavelengths in Figure 4B. The corresponding data for other excitation wavelengths are available in Supporting Information Fig. S3 & S4. Major differences are observed in the shapes of the kinetic traces and a multitude of different peaks and valleys is observed in the contour plot, both indicating that lycopene aggregates exhibit a highly complex dynamic behavior. Different bands not only appear, disappear and reappear at different timescales, they also exhibit spectral shifts, resulting in kinetic traces with as many as six different minima and maxima occurring at different delay times (see *e.g.* the induced absorption band at 327 nm).

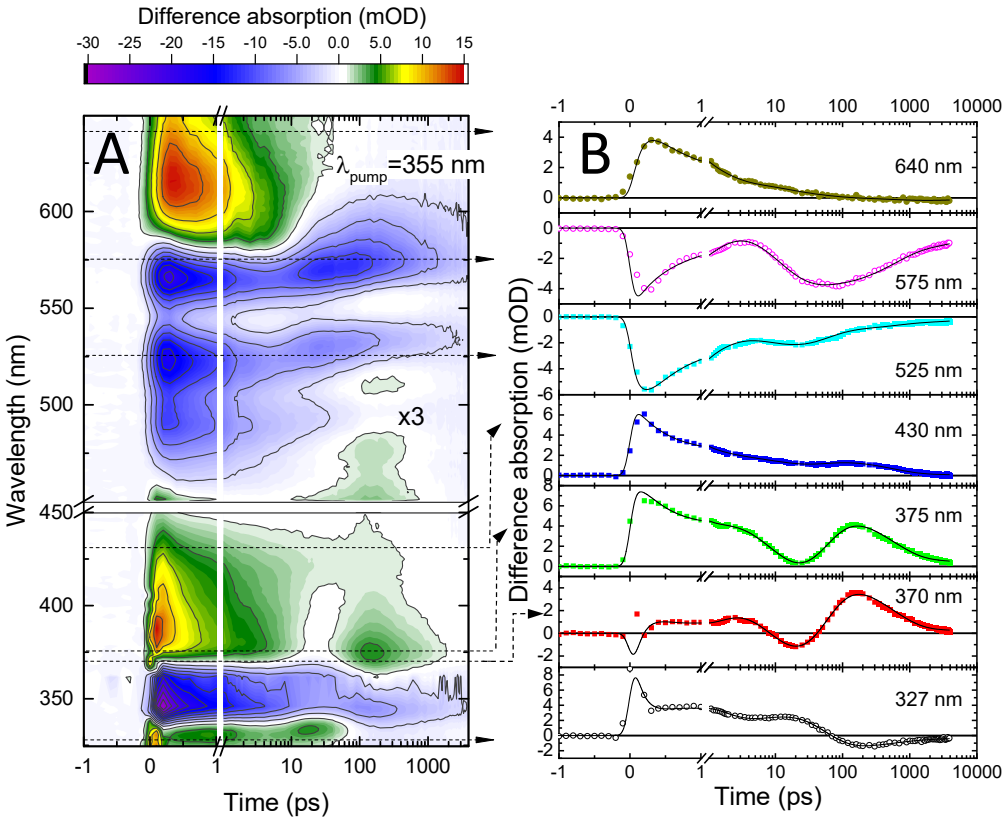

Figure 4 | Femtosecond-to-nanosecond transient absorption data of lycopene aggregates upon excitation at 355 nm. **A:** contour plot of the dataset. **B**: kinetic traces measured at different wavelengths (indicated on the graphs) along with the results of the global fit to the data (solid lines). Horizontal dashed lines in panel A indicate the wavelengths at which the kinetic traces were taken. Note that the signals measured above 450 nm were multiplied by a factor of 3 to aid viewing.

A more systematic data presentation is given in Figure 5A, where the same three datasets are plotted in the form of time-gated spectra and compared with evolution-associated difference spectra (EADS) – the latter resulting from a global fit of the data using a sequential kinetic scheme.

At first, observation of the datasets collected at three different excitation wavelengths suggests that the main features of the observed dynamics are similar for all three excitation wavelengths. However, significant differences are present in the details of decay kinetics and the intensity ratios of different bands. Let us first classify the different spectral regions by assigning them with names to aid the discussion of the dynamics in detail.

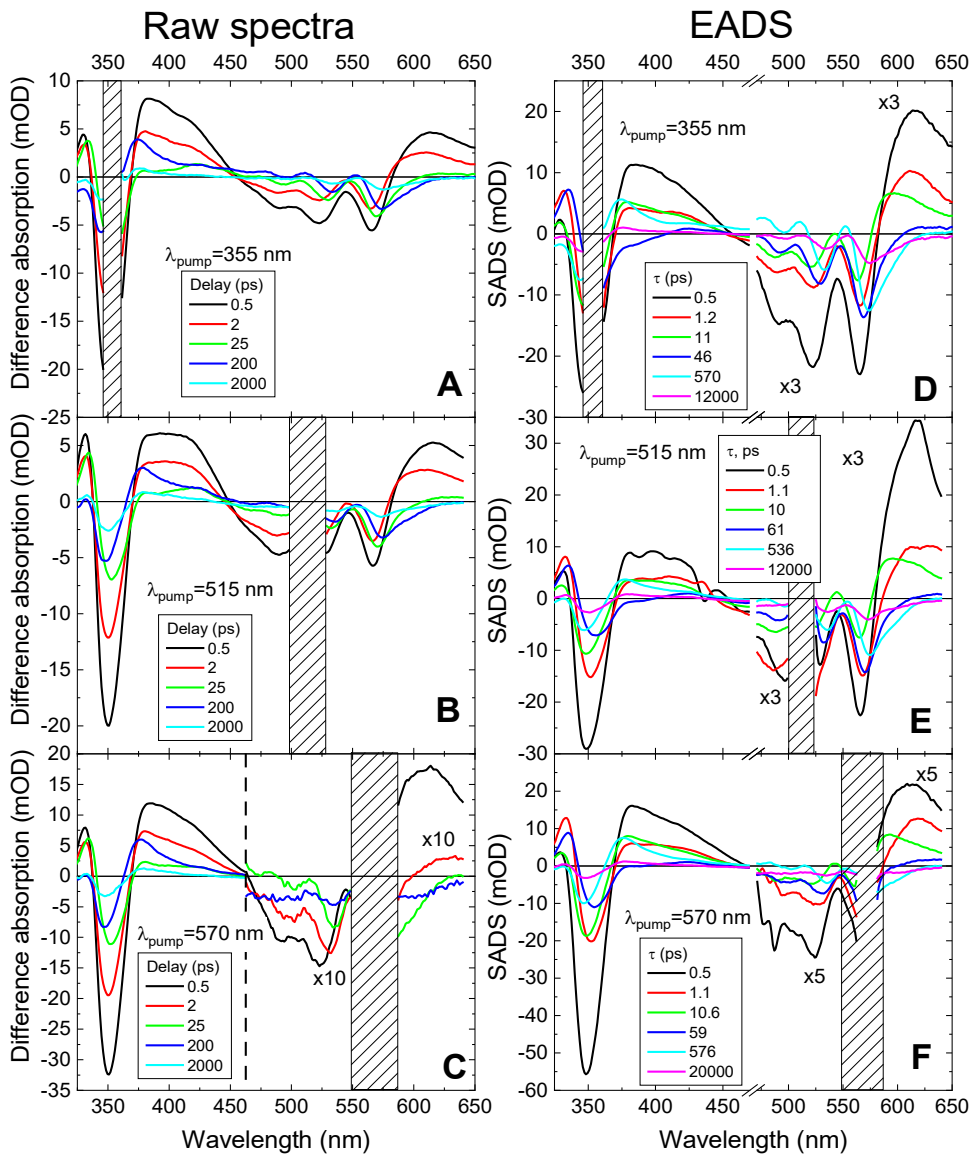

Figure 5| Dispersion-corrected time-gated pump-probe spectra of lycopene aggregates excited at 355 nm (**A**), 515 nm (**B**) and 570 nm (**C**). The times at which the spectra were taken are indicated on the graphs. Panels D, E and F show the EADS for the same datasets along with time constants, associated with different evolution steps, as *per* the legends.

Starting from the high energy side (Figure 5A, B, C), the difference spectra consist of an induced absorption (IA) band peaking around 330 nm (hereafter referred to as IA-330), and a ground state bleach (GSB) corresponding to the strong 355 nm absorption seen in the steady-state spectrum (denoted GSB-355). Further to the red, IA is again observed as a broad band stretching up to ca. 450 nm (IA-400), from where it is again replaced by a GSB signal exhibiting a clear vibronic-like structure - similar to the series of maxima observed in the red part of the absorption spectrum (GSB-550).

Finally, the early signals at wavelengths beyond 580 nm are dominated by IA, and replaced by long-lived negative signals (IA-GSB-600).

A detailed summary of the fs-ns transient absorption dynamics is presented in the form of EADS in Figure 5D, E and F. The presented spectra are a result of fitting the data to a sequential kinetic model ($A \rightarrow B \rightarrow C \rightarrow \ldots$). The error on the time constants in the ps range is of the order of 25%, and the last constant in the ns range cannot be estimated precisely due to the limited experimental time window. The spectrum of an initial component (lifetime of ca. 150 fs) was strongly contaminated by coherent-coupling artifacts, and was therefore omitted from the presentation. The quality of the fit can be assessed from the traces depicted in Figure 4B, and the similar data for other excitation wavelengths in supporting Information figures S3 & S4. We first note that the evolution time constants produced by the fitting are quite similar for all three datasets, allowing us to directly compare the spectra of different components between the three excitation wavelengths.

In the IA-300 region, the induced absorption band exhibits a 0.5-ps growth, and then decays almost to zero over the next 1.1 ps evolution step (see transition from black to red in Figure 5D, E, F). This is in contrast with all the other spectral regions (GSB-355, IA-400, GSB-550 and IA-GSB-600), where the absorption difference decays twofold in 0.5 ps, but in the subsequent 1.1 ps remains approximately constant, albeit with small spectral shifts. These shifts are best noticeable in the GSB-355 region, where the GSB maximum first shifts to the red, and then back to the blue. The spectral evolution on ca. 10-ps timescale produces the most dramatic spectral change (green-to-blue in Figure 5D, E, F). IA-330 reappears (slightly red-shifted compared to the 1.1-ps spectrum), while GSB-355 shifts noticeably to the red and develops a negative tail, replacing the initially-observed positive IA-400 with negative GSB (the latter is clearly discerned in the blue EADS at wavelengths up to 400 nm). This is accompanied by the disappearance of IA in the IA-GSB-600 spectral region, and the emergence of a negative GSB signal. Within ca. 50-60 ps, the blue EADS is replaced by cyan EADS, where – once again – most of IA-330 is lost, the negative peak of GSB-355 is again shifted to the blue, and IA-400 reappears, reminiscent of the signal observed at the 10 ps evolutionary step. In the GSB-550 region, the vibronic bands shift to the red, and the red GSB tail in the IA-GSB-600 range becomes more pronounced. The last step in spectral evolution is mostly the loss of signal amplitude. However, it also shifts the GSB-355 band to the red (again), loses almost all of the IA signal in the IA-400 region, and further red-shifts the GSB-550 vibronic-like bands and the red GSB tail in IA-GSB-600. This plethora of growths and decays, and shifts in both directions, results in the complicated spectro-

temporal picture shown in Figure 4. Note that unlike lycopene in solution but similarly to lycopene aggregates in films, we are left with long-lived absorption features with bleaching above 580 nm and at 355 nm, with an induced absorption band peaking at ca. 370 nm.

The amplitudes of the different bands exhibit an interesting feature for 570 nm excitation: the signals in GSB-500 and IA-GSB-600 are significantly weaker in this dataset, compared to excitation at 355 and 515 nm. This is obvious in Figure 5A, B and C, where the signals obtained at 570 nm (C) had to be multiplied by a factor of 5 to be readable on the same scale. This observation is counterintuitive in the context of both steady-state absorption and resonance Raman data, where both 570 and 355 nm bands seemed to be related with each other and different to the species absorbing at 515 nm.

Transient absorption spectra in the ns-to-μs range were obtained to determine the fate of the excitation energy at longer timescales, with excitation wavelengths at 355, 514 & 570 nm. An overview of the datasets, along with the calculated EADS and selected kinetic traces, are show in Figure 6 for 355, 514 & 570 nm excitation. These EADS were the result of global analysis using an evolutionary model, and reflect a cascade of events with the following time constants: 20 ns $\rightarrow$ 2.3 μs $\rightarrow$ 128 μs. The evolution of intermediate species is the same for all the excitation wavelengths (355, 514 & 570 nm). The first EADS at 20 ns (black spectra) is convolved with the excitation laser, so it has been fixed to the value obtained from the fs-to-ns experiments. It shows two negative features peaking below 400 nm and in the 510-800 nm region, both of which can be assigned to GSB, whereas a featureless EADS appears in the 410-510 nm region. The observed spectrum is similar to the final EADS of the femtosecond dataset. The band composition of the second and third EADS are identical, showing a negative region around 400 nm that can be attributed GSB of the strong absorption peak at 355 nm. In the 440-580 nm region, there is ESA with valleys at 480 and 520 nm, which may correspond to the 0-2 and 0-1 vibronic peaks of the $S_0 \rightarrow S_2$ electronic transitions, respectively. In monomeric lycopene, the $T_1 \rightarrow T_n$ transition presents an ESA maximum circa 520 nm and decays over 12 μs[49, 50]. The results for the lycopene aggregates suggest that there are at least two different triplet species formed. The species associated to the first EADS has been identified as a triplet in tomato chromoplasts.[23] The second triplet species (second, third EADS) resembles the triplets produced in monomeric lycopene by photosensitization.[50] The only significant difference observed here is the ground state bleaching band observed below 400 nm.

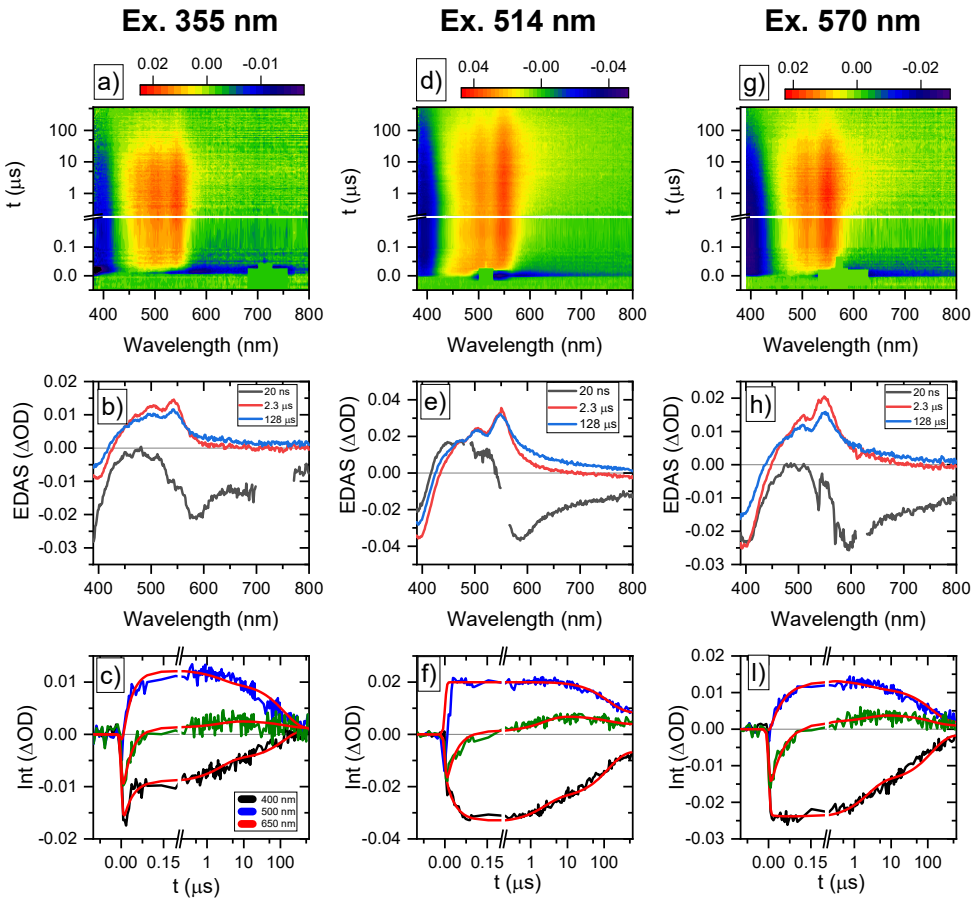

Figure 6| Nanosecond-to-microsecond transient absorption data of lycopene aggregates at 355, 515 and 570 nm excitation: a, d, g) dataset overview; b, e, h) EADS estimated by global fitting, using 3-component evolutionary model; c, f, i) selected kinetics and fitting.

Discussion

The data from resonance Raman measurements shows that the ν_1 frequency shifts with different excitation wavelengths, indicating that strong excitonic coupling between lycopene molecules affects the vibrational frequencies. From the analysis of the ν_1 and ν_2 regions, we observe that the sample contains at least four, and probably five species of lycopene aggregates. These observations are further supported by the complicated dynamics of femtosecond-to-nanosecond transient absorption. While it is, in principle, conceivable that a single type of aggregate or crystal could exhibit the number of evolutionary steps observed, it is hard to see how so many steps would result in the rise and fall of so many bands at more or less the same wavelengths. A more plausible explanation is that multiple types of aggregate are present in the sample with similarly (but not identically) positioned spectral bands, exhibiting overlapping dynamics.

Although relaxation schemes involving singlet fission have been proposed to explain the formation of triplets in astaxanthin and lutein/violaxanthin aggregates[13, 24], the current data seems too far from the established monomeric carotenoid dynamics to draw a straightforward connectivity scheme explaining all the experimental observations. The attempts at describing dynamics would first require a structural model that would reproduce the absorption spectrum in Figure 1B. More specifically, the presence of aggregate absorption bands both red-shifted and blue-shifted from the main transition should be carefully addressed. Traditionally, such bands are attributed to J- and H-aggregates, resulting from two different types of transition dipole orientations. The quasi-one-dimensional structure of the π-conjugated chain of carotenoid molecules determines the direction of their $S_0 \rightarrow S_2$ transition dipole along the molecular backbone. Hence, the two bands *must* result from (at least) two types of orientation (and therefore of coupling) of lycopene molecules in an aggregate. Both H- and J-type aggregates have been observed for astaxanthin [51], but they occur at different acetone-water ratios, allowing their separate investigation. Additionally, Fuciman *et al.* [29] have reported that two spectrally-distinct H-aggregates of astaxanthin can be formed, and both produce long-lived triplet states, presumably via singlet fission. In line with these observations, the presence of a heterogeneous mixture of similar types of aggregates in the lycopene assemblies presented here would explain why the observed spectroscopic behavior is so complex.

Assuming our multi-aggregation hypothesis is correct, the observed spectroscopic and spectro-temporal features are a result of the following physical phenomena, taking place in multiple aggregate types:

1. Different exciton dynamics and intramolecular vibrational energy redistribution (IVR) within a single aggregate type (including energy equilibration within the excitonically-coupled S_2 manifold), and subsequent relaxation to S_1, S* and other optically-dark states present in carotenoids. This would account for the redshifts of GSB bands, observed around 355 and 550-600 nm.
2. Vibrational cooling of the hot S_1 state, typically occurring in monomeric carotenoids on a sub-ps timescale [52], which manifests itself as a narrowing and blue-shift of the IA band peaking at ca, 570 nm in lycopene monomers.

3. Excitation energy transfer between the different aggregate types. This would decay the GSB bands characteristic of one aggregate type and induce bleaching of the other bands, resulting in the delayed appearance of GSB signals.
4. Singlet-fission, occurring with different efficiencies and at different rates in different aggregates, eventually resulting in triplet states. Depending on the details of this mechanism, singlet fission can result in the growth of GSB signals, when two triplet excitations are produced from a singlet.
5. Equilibration, including triplet energy transfer, and inhomogeneous decay of produced triplet states via internal conversion, triplet-triplet annihilation, etc.

We have already hypothesized three coexisting moieties with at least five (S_2, hot S_1, S_1, S*, T_1) interconnected excited states. This is more than enough to over-parametrize the datasets that are satisfactorily described by the 8 time constants (five in the fs-ns range plus three in the ns-µs range). The electronic signatures for the excited states are highly distorted from the well-characterized signatures for monomeric or weakly-interacting carotenoids. It is reasonable that the excited states experiment a similar degree of aggregation-associated spectral distortion as that seen for the ground states in the absorption spectrum. However, based on the lifetimes obtained it is tempting to propose a tentative assignment as follows: $<$ 500 fs EADS to S_2-like state, ca. 1p EADS to hot-S_1-like state, 10-11ps EADS to S_1-like state, 46-60ps EADS to S*-like state, which would then be the parent state for triplets, and the ca 550 ps EADS to interacting triplet states. It is clear that in order to better understand the spectroscopic properties of lycopene aggregates, it is necessary to design an alternative experimental protocol where each aggregate type can be observed selectively. This would allow us to propose more sophisticated models than the current linear scheme. The selective purification of each species of lycopene aggregate would clearly be ideal, but this may well turn out to be extremely complex given the number of different aggregate types formed here and reported in the literature. An alternative would be to use time-resolved resonance Raman spectroscopy, which should be sensitive enough to separate and distinguish the different excited states involved. Indeed, the selectivity of resonance Raman spectroscopy, and its sensitivity to the different arrangements of lycopene aggregates in their ground state, is illustrated very clearly in Figure 2. Whatever the case, the presence of several aggregation-domains, within the large lycopene aggregates observed by TEM, remains the best hypothesis to explain the obtained spectroscopic data.

Conclusions

We have successfully prepared stable aggregates of lycopene in an acetone-water mixture and investigated their absorption properties, resonance spectra, and ultrafast transient absorption dynamics. Our results reveal highly complex dynamics, involving spectral bathochromic and hypsochromic shifts, and the decay and reappearance of multiple spectral bands. Eventually, the dynamics result in long-lived triplet states formed *via* singlet-fission. We postulate that the dynamics are the result non-homogeneous aggregates, as observed by TEM, which contain multiple, connected subdomains of H-aggregates, each with their own set of excited state dynamics. If this hypothesis is validated by further structure-sensitive experiments, multi-aggregation may prove to be an essential factor in understanding the properties of other carotenoid aggregates.

Conflicts of interest

There are no conflicts to declare.

Acknowledgements

This work benefited from the Resonance Raman platform of I2BC, supported by the French Infrastructure for Integrated Structural Biology (FRISBI) ANR-10-INSB-05. The work was supported by the *Agence Nationale de la Recherche* (ANR), under the grant ANR-20-CE11-0022 (project EXCIT) and the CNRS as part of its 80PRIME interdisciplinary program.

References

1. G. Britton, S. Liaaen-Jensen and H. Pfander, *Carotenoids, Volume 4: Natural Functions*, Birkhäuser Verlag, Switzerland, 2008.

2. P. Tavan and K. Schulten, *Physical Review B*, 1987, **36**, 4337-4358.

3. M. J. Llansola-Portoles, A. A. Pascal and B. Robert, *Journal of The Royal Society Interface*, 2017, **14**.

4. M. M. Mendes-Pinto, E. Sansiaume, H. Hashimoto, A. A. Pascal, A. Gall and B. Robert, *J. Phys. Chem. B*, 2013, **117**, 11015-11021.

5. H. A. Frank and R. L. Christensen, in *Carotenoids: Volume 4: Natural Functions*, eds. G. Britton, S. Liaaen-Jensen and H. Pfander, Birkhäuser Basel, Basel, 2008, DOI: 10.1007/978-3-7643-7499-0_9, pp. 167-188.

6. H. A. Frank, A. J. Young, G. Britton and R. J. Cogdell, Kluwer Academic Publishing, 1999.

7. H. Hörvin Billsten, D. Zigmantas, V. Sundström and T. Polívka, *Chem. Phys. Lett.*, 2002, **355**, 465-470.

8. T. Polívka and V. Sundström, *Chem. Phys. Lett.*, 2009, **477**, 1-11.

9. T. Buckup and M. Motzkus, *Annu. Rev. Phys. Chem.*, 2014, **65**, 39-57.

10. V. Balevičius, D. Abramavicius, T. Polívka, A. Galestian Pour and J. Hauer, *J. Phys. Chem. Lett.*, 2016, **7**, 3347-3352.

11. A. E. Jailaubekov, M. Vengris, S.-H. Song, T. Kusumoto, H. Hashimoto and D. S. Larsen, *J. Phys. Chem. A*, 2011, **115**, 3905-3916.

12. A. Kundu and J. Dasgupta, *J. Phys. Chem. Lett.*, 2021, **12**, 1468-1474.

13. A. J. Musser, M. Maiuri, D. Brida, G. Cerullo, R. H. Friend and J. Clark, *J. Am. Chem. Soc.*, 2015, **137**, 5130-5139.

14. J. Zuo, L. Tan, Y. Xu, Y. Ma, J. Dong, P. Wang and J. Zhang, *Chem. Res. Chin. Univ.*, 2019, **35**, 627-635.

15. H.-T. Chang, Y.-Q. Chang, R.-M. Han, P. Wang, J.-P. Zhang and L. H. Skibsted, *J. Agric. Food Chem.*, 2017, **65**, 6058-6062.

16. D. Zhang, L. Tan, J. Dong, J. Yi, P. Wang and J. Zhang, *Chem. Res. Chin. Univ.*, 2018, **34**, 643-648.

17. C. Wang and M. J. Tauber, *J. Am. Chem. Soc.*, 2010, **132**, 13988-13991.

18. C. Wang, M. Angelella, C.-H. Kuo and M. J. Tauber, *Proceedings of SPIE*, 2012, **8459**, 05-13.

19. H. H. Billsten, V. Sundström and T. Polívka, *J. Phys. Chem. A*, 2005, **109**, 1521-1529.

20. C. C. Gradinaru, J. T. M. Kennis, E. Papagiannakis, I. H. M. van Stokkum, R. J. Cogdell, G. R. Fleming, R. A. Niederman and R. van Grondelle, *Proc. Natl. Acad. Sci.*, 2001, **98**, 2364-2369.

21. E. Papagiannakis, S. K. Das, A. Gall, I. H. M. van Stokkum, B. Robert, R. van Grondelle, H. A. Frank and J. T. M. Kennis, *J. Phys. Chem. B*, 2003, **107**, 5642-5649.

22. E. Papagiannakis, J. T. M. Kennis, I. H. M. van Stokkum, R. J. Cogdell and R. van Grondelle, *Proc. Natl. Acad. Sci.*, 2002, **99**, 6017-6022.

23. M. J. Llansola-Portoles, K. Redeckas, S. Streckaité, C. Ilioaia, A. A. Pascal, A. Telfer, M. Vengris, L. Valkunas and B. Robert, *Phys. Chem. Chem. Phys.*, 2018, **20**, 8640 - 8646.

24. A. Quaranta, A. Krieger-Liszkay, A. A. Pascal, F. Perreau, B. Robert, M. Vengris and M. J. Llansola-Portoles, *Phys. Chem. Chem. Phys.*, 2021, **23**, 4768-4776.

25. M. B. Smith and J. Michl, *Chem. Rev. (Washington, DC, U. S.)*, 2010, **110**, 6891-6936.

26. R. Pandya, Q. Gu, A. Cheminal, R. Y. S. Chen, E. P. Booker, R. Soucek, M. Schott, L. Legrand, F. Mathevet, N. C. Greenham, T. Barisien, A. J. Musser, A. W. Chin and A. Rao, *Chem*, 2020, **6**, 2826-2851.

27. R. Casillas, I. Papadopoulos, T. Ullrich, D. Thiel, A. Kunzmann and D. M. Guldi, *Energy & Environmental Science*, 2020, **13**, 2741-2804

28. C. Wang, D. E. Schlamadinger, V. Desai and M. J. Tauber, *ChemPhysChem*, 2011, **12**, 2891-2894.

29. M. Fuciman, M. Durchan, V. Šlouf, G. Keşan and T. Polívka, *Chem. Phys. Lett.*, 2013, **568-569**, 21-25.

30. A. V. Ruban, R. Berera, C. Ilioaia, I. H. M. van Stokkum, J. T. M. Kennis, A. A. Pascal, H. van Amerongen, B. Robert, P. Horton and R. van Grondelle, *Nature*, 2007, **450**, 575-578.

31. A. A. Pascal, Z. Liu, K. Broess, B. van Oort, H. van Amerongen, C. Wang, P. Horton, B. Robert, W. Chang and A. Ruban, *Nature*, 2005, **436**, 134-137.

32. M. Kasha, *Radiat. Res.*, 1963, **20**, 55-70.

33. N. J. Hestand and F. C. Spano, *Chem. Rev. (Washington, DC, U. S.)*, 2018, **118**, 7069-7163.

34. F. C. Spano, *J. Am. Chem. Soc.*, 2009, **131**, 4267-4278.

35. L. Lu, Y. Liu, L. Wei, F. Wu and Z. Xu, *J. Lumin.*, 2020, **222**, 117099.

36. J. Hempel, C. N. Schädle, S. Leptihn, R. Carle and R. M. Schweiggert, *Journal of Photochemistry and Photobiology A: Chemistry*, 2016, **317**, 161-174.

37. M. Ishigaki, P. Meksiarun, Y. Kitahama, L. Zhang, H. Hashimoto, T. Genkawa and Y. Ozaki, *J. Phys. Chem. B*, 2017, **121**, 8046-8057.

38. L. Wang, Z. Du, R. Li and D. Wu, *Dyes Pigm.*, 2005, **65**, 15-19.

39. J. Dong, D. Zhang, X.-Y. Wang and P. Wang, *Chem. Phys. Lett.*, 2018, **701**, 52-57.

40. V. R. Salares, N. M. Young, P. R. Carey and H. J. Bernstein, *J. Raman Spectrosc.*, 1977, **6**, 282-288.

41. C. Wang, C. J. Berg, C.-C. Hsu, B. A. Merrill and M. J. Tauber, *J. Phys. Chem. B*, 2012, **116**, 10617-10630.

42. S. Streckaite, M. Macernis, F. Li, E. Kuthanová Trsková, R. Litvin, C. Yang, A. A. Pascal, L. Valkunas, B. Robert and M. J. Llansola-Portoles, *J. Phys. Chem. A*, 2020, **124**, 2792-2801.

43. M. J. Llansola-Portoles, A. A. Pascal and B. Robert, in *Methods Enzymol.*, ed. E. T. Wurtzel, Academic Press, 2022, vol. 674, pp. 113-135.

44. Y. Koyama, I. Takatsuka, M. Nakata and M. Tasumi, *J. Raman Spectrosc.*, 1988, **19**, 37-49.

45. Y. Koyama, T. Takii, K. Saiki and K. Tsukida, *Photobiochem. Photobiophys.*, 1983, **5**, 139–150.

46. Y. Koyama, M. Kito, T. Takii, K. Saiki, K. Tsukida and J. Yamashita, *Biochim. Biophys. Acta, Bioenerg.*, 1982, **680**, 109-118.

47. L. Rimai, M. E. Heyde and D. Gill, *J. Am. Chem. Soc.*, 1973, **95**, 4493-4501.

48. M. Lutz, W. Szponarski, G. Berger, B. Robert and J.-M. Neumann *Biochem. Biophys. Acta*, 1987, **894**, 423-433.

49. M. Burke, E. J. Land, D. J. McGarvey and T. G. Truscott, *J. Photochem. Photobiol., B*, 2000, **59**, 132-138.

50. E. J. Land, A. Sykey and T. T. G., *Photochem. Photobiol.*, 1971, **13**, 311-320.

51. C. Köpsel, H. Möltgen, H. Schuch, H. Auweter, K. Kleinermanns, H.-D. Martin and H. Bettermann, *J. Mol. Struct.*, 2005, **750**, 109-115.

52. F. L. de Weerd, I. H. M. van Stokkum and R. van Grondelle, *Chem. Phys. Lett.*, 2002, **354**, 38-43.